

Article

Not peer-reviewed version

Modelling the Cost-Effectiveness of PV Module Replacement Based on a Quantitative Assessment of Defect Power Loss

[Victoria Lofstad-Lie](#)*, [Bjørn Lupton Aarseth](#), [Nathan Roosloot](#), [Erik Stensrud Marstein](#), [Torbjørn Skauli](#)

Posted Date: 12 October 2024

doi: 10.20944/preprints202410.0928.v1

Keywords: PV module defects; PV module degradation; PV module power loss; thermal imaging; electroluminescence imaging; light IV








Preprints.org is a free multidisciplinary platform providing preprint service that is dedicated to making early versions of research outputs permanently available and citable. Preprints posted at Preprints.org appear in Web of Science, Crossref, Google Scholar, Scilit, Europe PMC.

Copyright: This open access article is published under a Creative Commons CC BY 4.0 license, which permit the free download, distribution, and reuse, provided that the author and preprint are cited in any reuse.

Article

Modelling the Cost-Effectiveness of PV Module Replacement Based on a Quantitative Assessment of Defect Power Loss

Victoria Lofstad-Lie ^{1,*} , Bjørn Lupton Aarseth ² , Nathan Roosloot ^{1,2} , Erik Stensrud Marstein ^{1,2} , and Torbjørn Skauli ^{1,3} 

¹ Department of Technology Systems, University of Oslo, 2007 Kjeller, Norway

² Institute for Energy Technology (IFE), 2007 Kjeller, Norway

³ Norwegian Defence Research Establishment, 2007 Kjeller, Norway

* Correspondence: victoria.lofstad-lie@its.uio.no

Abstract: The degradation of solar photovoltaic (PV) modules over time, aggravated by defects, significantly affects the performance of utility-scale PV parks. This study presents a quantitative assessment of the power loss from module defects, and evaluates the cost-effectiveness of replacing defective modules at various stages of degradation. A module test site was established in Norway with six different defects, and continuous thermographic monitoring, combined with light IV measurements and electroluminescence (EL) imaging, provides partial support for further calculations on the long-term effects of the defects. The cumulative module energy loss is calculated over a 25-year park lifespan under both Norwegian and Chilean environmental conditions, the latter representing higher solar irradiation levels. The energy gain from replacing the defective modules at various stages of degradation is compared to the costs of replacement, both for infant-life failures and mid-life failures. Minor infant-life defects of 1% power loss are likely not beneficial to replace in low-irradiation regions like Norway. For Chilean conditions it can be cost-effective, but primarily if the module is replaced around mid park life, which gives a larger yield when replaced with a new module. For more severe defects of 10% loss the replacement gain is above the replacement cost for high-irradiation locations, and replacing the 33% power loss defect is cost-effective for both locations, even when discovered late in the park lifetime. Mid-life defects are primarily beneficial to replace in high-irradiation locations.

Keywords: PV module defects; PV module degradation; PV module power loss; thermal imaging; electroluminescence imaging; light IV

1. Introduction

Solar photovoltaic (PV) technology has become one of the leading renewable energy resources due to technological advancements and a significant reduction in power generation costs [1]. Between 2010 and 2022, the global average cost of electricity generation from large-scale PV plants decreased by nearly 89% [2]. However, as PV systems age, the degradation of modules and the emergence of defects become critical factors that affect their long-term performance, reliability, and economic viability [3].

Module defects, such as hot spots, cracks, or defective bypass diodes, can lead to considerable power losses over time, reducing the overall efficiency of the system [4]. Detecting these defects and quantifying their impact on power output is essential for effective operation and maintenance (O&M) strategies. Accurate defect identification allows operators to make informed decisions about when to repair or replace defective modules, ensuring maximum energy yield and return on investment (ROI).

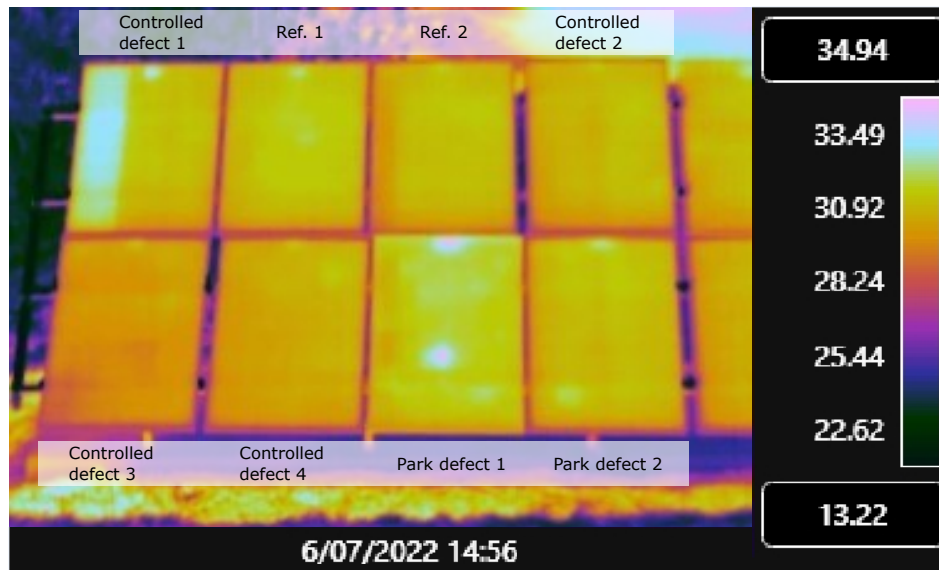


Figure 1. Thermal image of the module test site. The "Controlled defects" are deliberately created, and consist of a bypassed substring (Controlled defect 1), and cell cracks (Controlled defect 2 to 4). The "Park defects" are collected from a solar park, and have cell hotspots. Ref. 1 and 2 are reference modules. The image is taken at a solar irradiance of 600 W/m^2 in the module plane.

This paper presents a quantitative assessment of power losses due to defects in PV modules, focusing on the cost-effectiveness of module replacement. The study was initiated as an experiment where a module test site was established, and the modules were characterized during lab tests and with thermography. The measurements from the module test site form the foundation for further calculations on the cumulative power loss during a 25 years park life, taken into account a general module degradation, as well as a deterioration of the defects. Finally, the energy gain associated with replacing defective modules is presented at different stages of degradation, both for defects appearing early in the park lifespan, and defects appearing mid-life. The study examines how environmental factors, such as solar irradiation, influence the defect loss, comparing results from the test site in Norway with simulated conditions in Chile — a location with significantly higher solar irradiation. The energy gain is compared to the cost of replacing the modules, which determines if, and when, replacement is the cost-effective O&M measure.

2. Module Degradation - A Brief Review

Module degradation refers to a gradual decline in the performance while still meeting the warranty requirements [5]. Examples of degradation modes are encapsulant discoloration, delamination, and ribbon discoloration. Environmental factors, such as high UV irradiation, humidity, and temperature, have been identified as significant contributors to the degradation process [6]. Studies describe higher degradation rates in hotter climates compared to more moderate climates [7,8]. In [9], the authors explore the degradation rates in four climate zones based on the Köppen-Geiger classification, and find a median degradation rate of around 0.9% in desert climate, 0.5% in hot & humid climate, 0.7% in moderate climate, and 0.5% in climates with snow.

In addition to the gradual module degradation from exposure to the elements, it has been reported that defects might deteriorate with time, causing an additional degradation of defective modules [10]. In [11], the authors find that modules with cracked cells degraded in the field with an average of 0.5% more than uncracked modules over a period of 21 months, which corresponds to a yearly additional degradation of 0.3% for the cracked modules. The authors in [12] compare the degradation rates of 60 healthy modules with 40 modules with hotspots operating over 10 - 17 years in a desert climatic condition of Arizona. In the absence of intermittent performance data on the individual modules, the degradation rate is assumed to be linear, yielding an increase in the degradation rate of 0.46% - 3.3%

per year in the modules with hotspots compared to the non-defective modules for different models. On average, the 35 defective p-Si modules in the experiment had an elevated degradation of 0.8% compared to the non-defective. While most studies done on the degradation of defective modules typically assume a linear degradation rate, the authors in [13] suggest that the fault degradation might follow other curves than a linear degradation. A module exhibiting cracks in the cell and the string interconnect ribbons degraded 12% over a period of ten years, following a curve shown in Figure A1 in Appendix A. The authors found a degradation following the exponential function $y(t) = 0.181 \cdot (1.055^t - 1)$ where t is time in years. The defect degradation is not compared to the non-defective module degradation, so in further analyses the exponential function will represent the total degradation. [14] found no evolution of cracks after one year of outdoor exposure.

In this article, we will differentiate between module degradation and defect degradation, and treat them as additive effects. We will refer to module degradation as the median degradation exhibited by all PV modules in the power plant, and defect degradation as the additional degradation exhibited by PV modules with observed defects. The analyses will explore the energy loss from defective modules located in Norway and Chile. Norway falls in the "snow" climate in [9], so a module degradation of 0.5% will be used, while Chile classifies as "desert" climate, with the associated median degradation rate of 0.9%. The module degradation and defect degradation in the mentioned literature are summarised in Figure 2 for a) Norway and b) Chile. As with the module degradation, the defect degradation rate might also depend on the climatic zone. However, lack of publications of the topic limits this study to assume the same defect degradation in Norway and Chile.

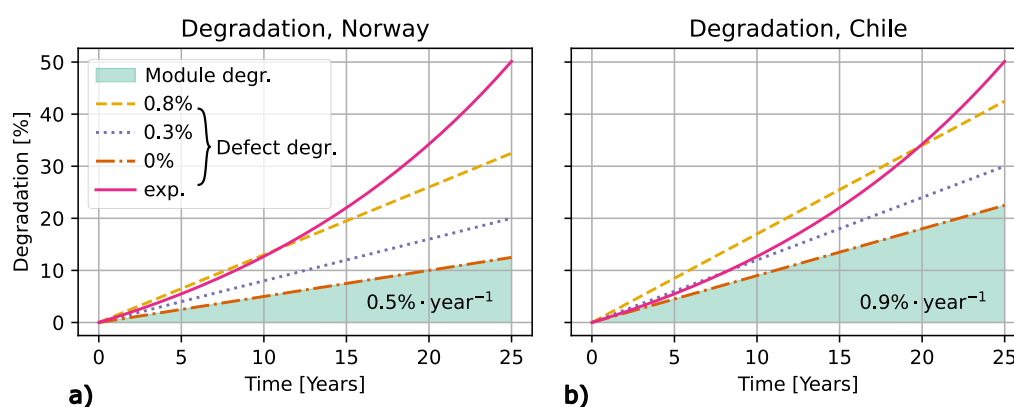


Figure 2. The average module degradation rate is plotted in green for a) Norway and b) for Chile. Additionally, four different defect degradation rates are added to the general module degradation. The exponential defect degradation is not separated from the module degradation, and is therefore the same for both locations.

3. Experimental

A module test site with six defective c-Si modules, as well as two reference modules, was established at Kjeller (60°N), Norway, for continuous thermographic monitoring and periodic lab characterization. The module setup is shown in infrared in Figure 1. The modules named Park defect 1 and 2 have cell hotspots that were discovered during operational monitoring. The modules were produced in 2012, and are collected from Glava Energy Center in Sweden. The module named Controlled defect 1 - 4 have defects deliberately created by the authors. Controlled defect 1 has an open-circuit substring resulting from cutting the connection to one of the cell strings, which is equivalent to a situation where the bypass diode is activated. A reference module of the same type is shown as Ref. 1. Controlled defect 2 - 4 have cell cracks that were created by damaging selected cells using a hammer on the backside of the module, and imitate failures caused by mechanical stress or manufacturing issues. The corresponding reference module is denoted as Ref. 2. All the modules

are connected in series, but with individual optimizers, meaning that each module operates at its maximum power point independently of each other.

All modules were characterized with light IV measurements on August 26th 2020. The measurements were performed with a Spi-Sun 5100 Single Long Pulse (SLP) solar simulator with an A+A+A+ rating according to [15], and a repeatability of 0.3%. Light IV is used to measure electrical properties like the maximum power P_{\max} at standard test conditions (STC) of 1000 W/m². Additionally, electroluminescence imaging of the modules was performed on the same day. For Controlled defect 1 - 4, the light IV measurements and electroluminescence imaging were performed before and after the damage was inflicted to the modules to assess the effect of the defects.

A Flir A325 radiometric thermal camera with a resolution of 320 x 240 pixels was permanently installed on an adjacent rooftop. The camera imaged the module test site every minute during the following time intervals:

- 2020: August 27th to September 9th, October 1st to 8th
- 2021: May 5th to September 9th
- 2022: May 19th to June 8th

Additionally, a weather station measured the solar irradiance in the module plane every five minutes.

4. Methodology

4.1. Clear-Sky Filtering of Thermography Images

Photovoltaic Library (PVLIB) [16] was used to model the clear-sky Global Horizontal Irradiance (GHI) at the solar array's location, which was compared to the irradiation measured on-site. Clear-sky conditions were determined when the deviation between the measurements and the model was below 10%. This threshold value was determined from manual testing and inspection. Additionally, to achieve steady-state conditions, a continuous duration of clear-sky conditions for at least 10 minutes was required. Only periods of clear-sky and steady-state conditions are used for the thermography analysis. Figure 3 illustrates the filtering, where the modeled and measured GHI is in purple and red, respectively. The green areas indicated clear-sky and steady-state conditions, while the yellow areas indicate that clear-sky conditions are met, but a thermal steady-state is not yet achieved.

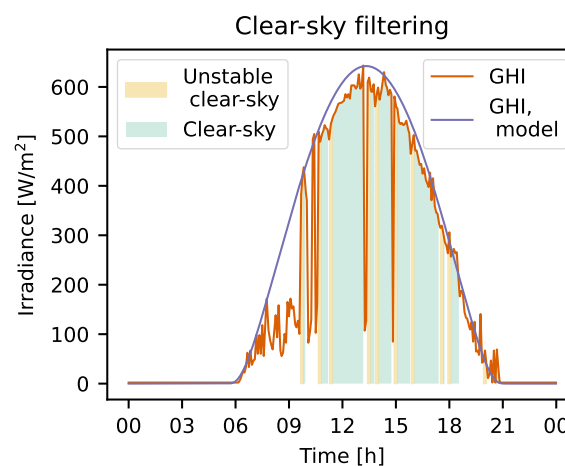


Figure 3. The measured Global Horizontal Irradiance (GHI) at the test site is shown in red, and the modeled GHI in purple. Clear-sky conditions are highlighted in green, and clear-sky conditions that have not yet reached steady-state are depicted in yellow, labeled as 'Unstable clear-sky'.

4.2. Defect Heating and Power Loss

The temperature difference between a defect and a healthy module is denoted ΔT , and represents a key parameter to determine the type and severity of a defect from thermal images. In steady-state

conditions, ΔT acts as proportional to the power loss ΔP caused by internal defects in a module, as dictated by the energy balance, where the additional internal losses are dissipated as heat in accordance with the conservation of energy [17]. With ΔT as the temperature difference between a defective and non-defective module, this can be expressed as

$$\Delta T = k \cdot \Delta P \quad (1)$$

where k is the proportionality constant. Due to the low lateral thermal conductivity of a module, the heating tends to be localized to the defective cells. It then follows that the temperature difference ΔT_{cell} between the defective cells and the non-defective area is

$$\Delta T_{\text{cell}} \cdot A = k \cdot \Delta P \quad (2)$$

where A is the area of the defective cells.

4.3. Cumulative Energy Loss from Defects and Degradation

The defect heating ΔT is often assumed proportional with the irradiance G [18,19], which Figure 5 b) supports as a fair assumption, where the ΔT of a bypassed substring is plotted against irradiation, showing a linear correlation. The relation between standard test conditions STC and inspection conditions $insp.$ is therefore described as $\Delta T_{\text{insp.}} / \Delta T_{\text{STC}} = G_{\text{insp.}} / G_{\text{STC}}$. Combined with Equation (1), it follows that the defect power loss ΔP_{defect} at the irradiance $G_{\text{insp.}}$ can be described as

$$\Delta P_{\text{defect}} = \frac{G_{\text{insp.}}}{G_{\text{STC}}} \cdot \Delta P_{\text{STC}} \quad (3)$$

If the relative amount of degradation is a linear rate d_m per year, then the module degradation after t years at irradiance levels of $G_{\text{insp.}}$ can be expressed as

$$\Delta P_{\text{degr., mod}} = \frac{G_{\text{insp.}}}{G_{\text{STC}}} \cdot P_{\text{max}} \cdot d_m \cdot t \quad (4)$$

where P_{max} is the power production at STC of a defect-free module. The final contribution to degradation is the deterioration of defects, generally expressed to

$$\Delta P_{\text{degr., defect}} = \frac{G_{\text{insp.}}}{G_{\text{STC}}} \cdot P_{\text{max}} \cdot y(t) \quad (5)$$

where $y(t)$ in this work will vary according to the defect degradation rates in Table 2. With these three contributions to the total power reduction, the cumulative energy loss after τ years can be found with

$$E_{\text{loss}} = \int_0^{\tau} \Delta P_{\text{tot}} dt = \overline{\frac{G_{\text{insp.}}}{G_{\text{STC}}}} \cdot \int_0^{\tau} \left(\Delta P_{\text{STC}} + P_{\text{max}} (d_m \cdot t + y(t)) \right) dt \quad (6)$$

where $\overline{\frac{G_{\text{insp.}}}{G_{\text{STC}}}}$ is the average irradiation over time τ .

4.4. Energy Gain from Module Replacement

With the cumulative module energy loss from Equation (6), the energy gain from module replacement at time t_r can be calculated by comparing a scenario in which the defective module remains in

place with one where it is replaced, and integrating the difference with respect to replacement time t_r through a nominal 25-year lifetime:

$$E_{\text{gain}} = \int_{t_r}^{25} (\Delta P_{\text{tot}}(t) - \Delta P_{\text{degr., mod}}(t - t_r)) dt \quad (7)$$

which, for the linear defect degradation rates of d_d , is written out as

$$E_{\text{gain, lin.}} = \frac{\overline{G_{\text{insp.}}}}{G_{\text{STC}}} \cdot \int_{t_r}^{25} (\Delta P_{\text{STC}} + P_{\text{max}}(d_m + d_d) \cdot t - P_{\text{max}}d_m(t - t_r)) dt \quad (8)$$

and for the exponential defect degradation rate is written out as

$$E_{\text{gain, exp.}} = \frac{\overline{G_{\text{insp.}}}}{G_{\text{STC}}} \cdot \int_{t_r}^{25} (\Delta P_{\text{STC}} + P_{\text{max}} 0.181 \cdot (1.055^t - 1) - P_{\text{max}}d_m(t - t_r)) dt \quad (9)$$

5. Experimental Foundation

5.1. Characterization of Defects with Light IV and EL

The controlled defects were characterized with light IV measurements and EL imaging before and after damage was induced in 2020 to determine the impact of the defects. The EL images of the damaged cells are shown in Figure 4 for a) Controlled defect 2, b) Controlled defect 3, and c) Controlled defect 4. The images reveal the presence of dark spots and lines, indicating inactive cell areas and cracks in all three modules at locations consistent with the sustained impact.

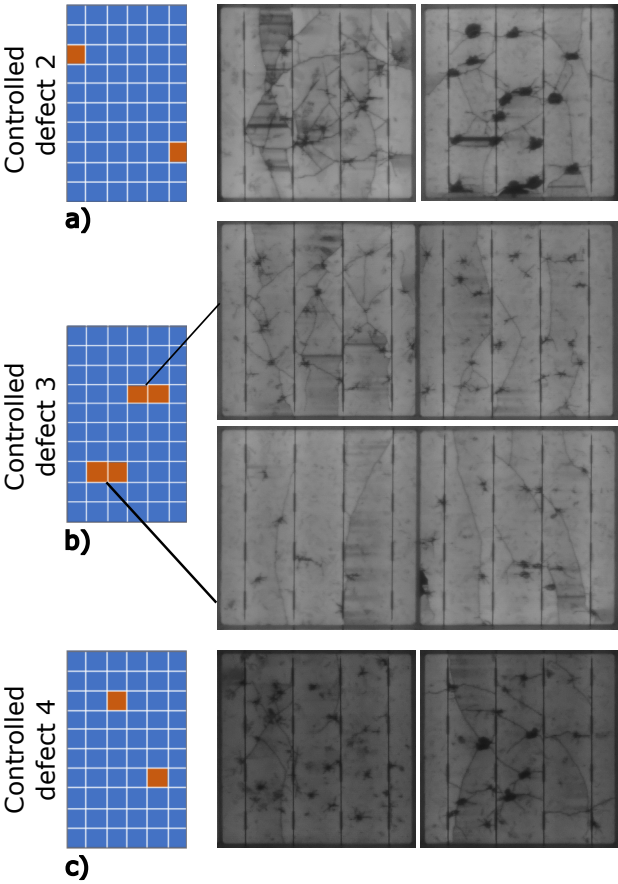


Figure 4. Electroluminescence images of the inflicted cell damage in a) Controlled defect 2, b) Controlled defect 3, and c) Controlled defect 4.

The change in the module maximum power P_{\max} was measured with light IV measurements under standard test conditions: Table 1 shows the P_{\max} for Controlled defect 1 - 4, measured before and after damage was inflicted ("Initial P_{\max} " and " P_{\max} post damage") in 2020. Controlled defect 3, with its four impacted cells, exhibited the largest drop of -1.6%, while Controlled defect 2 has a measured positive change of 0.7% despite the damage seen from EL. The increase is within the measurement uncertainty of 0.3%, and does most likely not represent an actual improvement in the module's performance. The bypassed substring in Controlled defect 1 caused a power reduction of 35%, close to the expected 33% drop.

Table 1. Maximum power from light IV measurements at standard test conditions before and after inflicted module damage.

Module	Initial P_{\max} [W]	P_{\max} post damage [W]	ΔP [W]	Relative change
Contr. defect 1	270.5	175.8	-95	-35%
Contr. defect 2	270.4	272.2	1.8	0.7%
Contr. defect 3	274.4	270.1	-4.3	-1.6%
Contr. defect 4	269.5	268.2	-1.3	-0.5%

5.2. Power Loss from Park Defects

While the lab induced defects are associated with a known power loss, the loss from the park defects is unknown. The power loss can however be assessed from the thermal images by using the bypassed substring in Controlled defect 1 as a reference for the relation between defect heating and power loss. With a known power loss of ΔP_{d1} , and the corresponding ΔT_{d1} available from the thermal

images, we can find the proportionality constant between ΔP_{d1} and ΔT_{d1} , denoted k in Equation (2). This can in turn be used to approximate ΔP for the other modules based on their measured ΔT . We know that the power loss ΔP_{d1} due to the substring failure is 95 W (see Table 1) when exposed to standard test conditions of 1000 W/m². From the thermal images captured at the same irradiance, we can calculate the heating of the bypassed substring compared to the two functioning substrings at the same module as a measure of ΔT_{d1} . 1131 images were captured at an irradiance of 1000±20 W/m² during steady-state conditions, yielding

$$\Delta T_{d1} = 3.1 \pm 1.2 \text{ K} \quad (10)$$

where 3.1 K is the average value and 1.2 K is the standard deviation. With a defect area of 20 cells, it follows from Equation (2) that

$$k = \frac{\Delta T_{d1} \cdot A}{\Delta P_{d1}} = \frac{3.1 \text{ K} \cdot 20 \text{ cells}}{95 \text{ W}} = 0.65 \frac{\text{K} \cdot \text{cells}}{\text{W}} \quad (11)$$

which gives the proportionality constant between ΔT and ΔP at 1000 W/m². With all modules exposed to the same conditions, we can apply k to the ΔP calculations of the remaining modules, keeping in mind that different module models makes this an approximation. The ΔT value of the park defects is obtained from the thermal images: 14 754 thermal images were taken during clear-sky conditions (the clear-sky filtering process is described in Sec. 4.1). As there are no reference modules of the same model as Controlled defect 1, ΔT is calculated by finding the mean temperature of the substring containing the hotspot (denoted " T_2 " in Figure 5 a), and subtracting the mean temperature of the remaining two substrings in the module (denoted " T_1 " and " T_3 "). The obtained $\Delta T_{subs.}$ is plotted against irradiation in Figure 5. At 1000 W/m², we obtain $\Delta T_{subs.} = 0.76 \text{ K}$. This can be used to calculate the corresponding energy loss at 1000 W/m², using Equation (2), where $A = 18$ cells because we exclude the two cells in the substring affected by the heated bypassed diode (as shown in Figure 5 a)):

$$\Delta P = \frac{\Delta T \cdot A}{k} = \frac{0.76 \text{ K} \cdot 18 \text{ cells}}{0.65 \text{ K} \cdot \text{cells} \cdot \text{W}^{-1}} = 21 \text{ W} \quad (12)$$

This fits well with the characterizations of the module: The module was originally rated with a peak power of $P_{\max} = 245 \text{ W}$ in 2012, and 211 W in 2023. This reduction in performance of 34 W is likely caused by a combination of the defect, calculated to 21 W, and degradation. The yearly degradation rate can not be determined due to an unknown combination of storage and use since 2012.

As for Park defect 2, the heating of the hot spot is insufficient to be distinguished from noise.

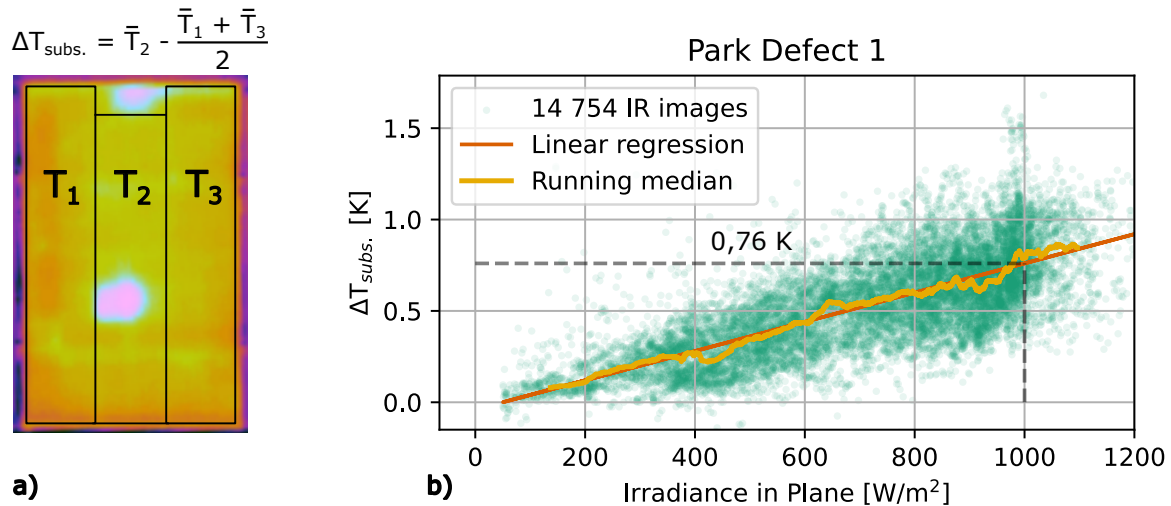


Figure 5. a): Park defect 1. The mean temperature of each substring is used to calculate $\Delta T_{subs.}$, here defined as the temperature difference between the substring with an hotspot, minus the mean temperature of the remaining two substrings. The calculations are shown above the module. b): The obtained $\Delta T_{subs.}$ values for Park defect 1 are plotted against the irradiance. The running mean and a linear regression with $R^2=0.53$ are shown.

6. Calculations on the Economic Impact of Defects

6.1. Cumulative Power Loss

With the module and defect degradation rates from Sec. 2, and defect losses from Sec. 5.1 and 5.2, the cumulative power loss is estimated with the calculations from Sec. 4.3, both for Norwegian and Chilean conditions. The required irradiance data was gathered from the module test site in Norway and from [20] for Chile. The calculations will assume a park lifetime of 25 years, complying with standard warranty periods, and assume that the defects are present from time $t = 0$. The P_{max} values are found as "Initial P_{max} " in Table 1 (here assuming that the values represent new modules) for the controlled defects, and the measured $P_{max} = 211$ W for Park defect 1.

To contextualize the energy loss, we compare it to the amount of energy a PV park operator must produce to offset the costs associated with module replacement. Both the cost of module replacement and the feed-in tariff price per kWh will vary with location and park size. The wholesale cost rate of a PV module is reported to be around 0.22€/W [21], constituting around 60€ for the 270 W modules in this study. We therefore assume a module replacement cost of 100 €/module, which also includes the installation and other related costs. For simplicity, in the calculation of income losses we assume that the income from PV power production is based on a fixed feed-in tariff. We investigate three different prices: 0.05, 0.1, and 0.5 €/kWh [22]. With these assumptions, the cost of module replacement is covered by the production of 2000 kWh, 1000 kWh, and 200 kWh, respectively. This is plotted together with the energy loss as "Replacement cost threshold".

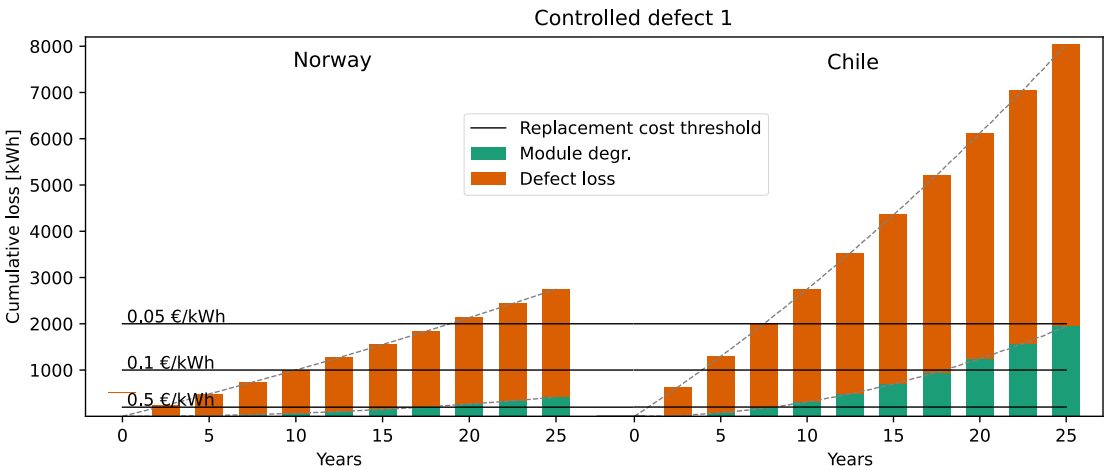


Figure 6. Cumulative power loss from Controlled defect 1 (bypassed substring) for conditions representative for Norway (left) and Chile (right).

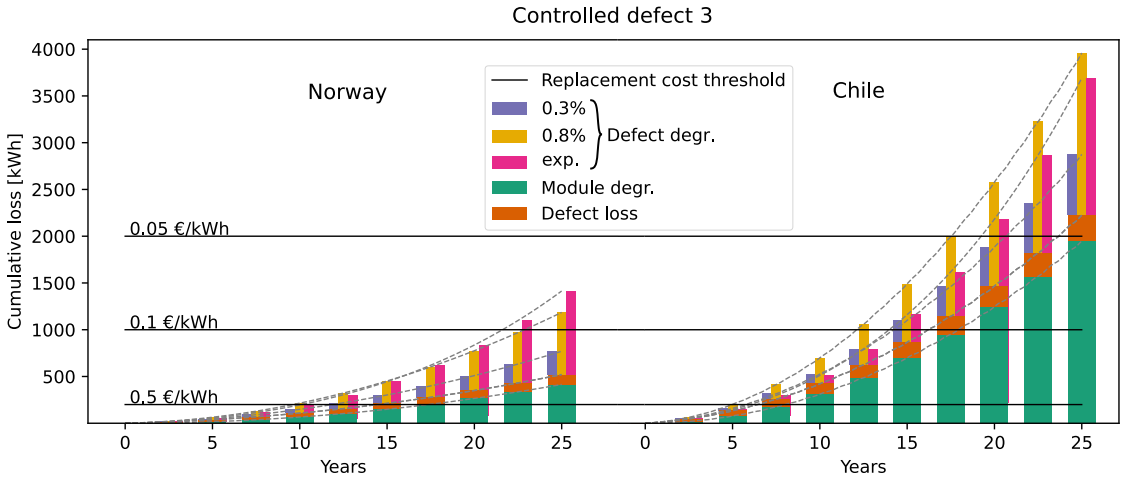


Figure 7. Cumulative power loss from Controlled defect 3 (cell cracks) for conditions representative for Norway (left) and Chile (right).

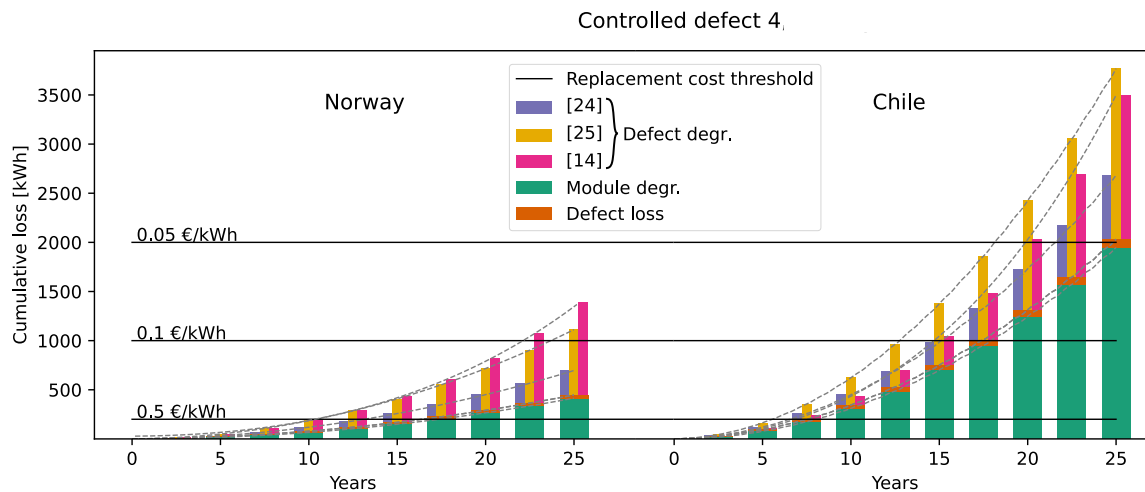


Figure 8. Cumulative power loss from Controlled defect 4 (cell cracks) for conditions representative for Norway (left) and Chile (right).

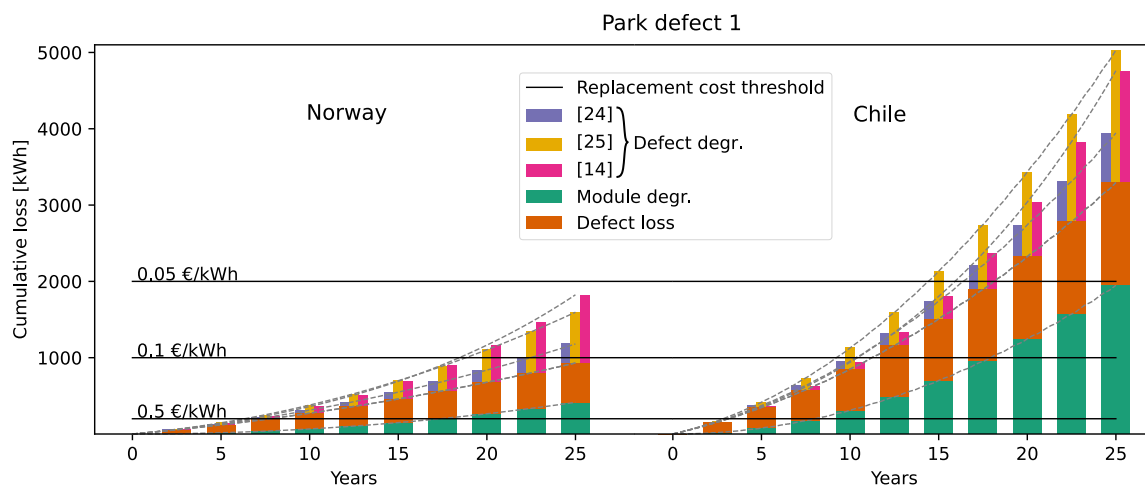


Figure 9. Cumulative power loss from Park defect 1 (hotspot) for conditions representative for Norway (left) and Chile (right).

Figure 6 shows the cumulative energy loss from the bypassed substring in Controlled defect 1. We assume that the diode is not degrading, so no additional defect degradation is added to the power loss. The figure shows that the defect loss dominates over the module degradation loss. Figure 6, 7, and 8 show the cumulative energy loss from Controlled defect 3, 4, and Field defect 1, respectively. The four different defect degradation rates are shown side-by-side in the bar plot for comparison, where the fourth rate is a defect degradation of 0%. The figures demonstrate that degradation loss is the dominant factor for these smaller defects. Overall, the cumulative loss in Chile is more than double that in Norway, driven by both higher power production and a greater module degradation rate. Under Chilean conditions, the energy loss from all four modules exceeds the yield needed to cover the cost of module replacement at all three feed-in tariff levels. While the figures indicate that the energy loss from defective modules may surpass the energy required to offset replacement costs, they do not reveal the optimal timing for replacement. If a module is replaced at $t = 0$, it will still degrade along the curve shown by the green bars, whereas replacing the module at $t = 12.5$ years will reset the degradation. The optimal timing for module replacement will be examined in the next section.

Table 2. Reported module degradation rates typical for the climates in Chile and Norway, and different defect degradation rates found in literature.

Type of degradation	Degradation rate per year	
Module degradation	Chile	0.9%
	Norway	0.5%
Defect degradation	[14]	0%
	[11]	0.3%
	[12]	0.8%
	[13]	Increasing: $0.181 \cdot (1.055^t - 1)$ where t is time in years

6.2. Module Replacement Gain

6.2.1. Infant-Life Failures

We will here calculate the energy gain from replacing defective modules at various points throughout the park's 25-year lifespan. This is illustrated in Figure 10 for different scenarios: a) shows a non-defective module that degrades with time, where module replacement at time t_r results in the energy gain shown in the green area. In b), the defect ΔP degrades with three different linear degradation rates until module replacement at time t_r , after which they degrade with the module degradation rate. c) shows the exponential degradation of a defect ΔP , and the gain from replacing it at time t_r . The gain can be calculated for varying t_r by solving the integral of the degrading defective module minus the degrading non-defective module from time t_r and to the end of the park life, as described in Sec. 4.4.

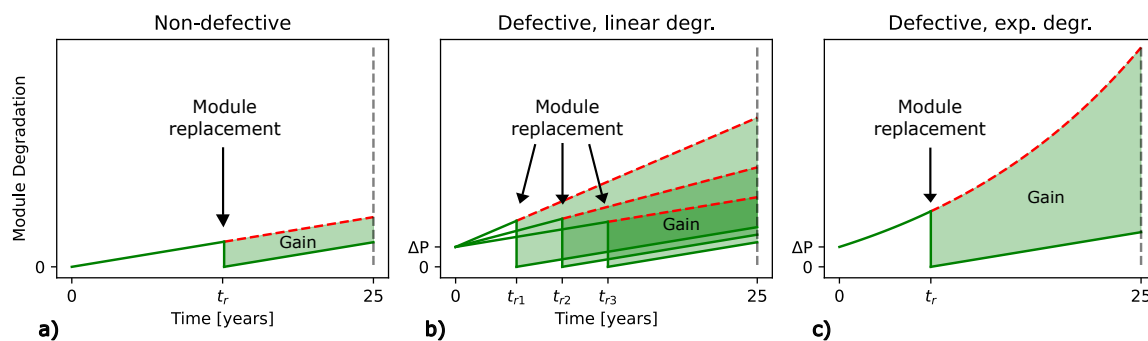


Figure 10. Illustration of the module degradation for a) a non-defective module, b) a defect with a loss of ΔP and three different linear defect degradation rates, and c) a defect ΔP with an exponential degradation. The green areas illustrate the gain from module replacement at time t_r .

The gain will be compared with the same break-even thresholds as in previous section to determine if the energy gain from module replacement is higher than the cost of replacement, and therefore a cost-effective measure. The calculations assume that the defects are present from the beginning of the park lifetime, imitating infant-life failures defects arising from e.g., manufacturing, transportation, or installation. The same degradation rates as in previous section will be used, presented in Table 2, and three different defect losses of 1%, 10%, and 33% of the initial module P_{\max} . The 1% defect represents the inflicted cell damage in Controlled defect 3 and 4, the 10% defect is of the same severity as the Park defect 1, and the 33% defect represents the bypassed substring in Controlled defect 1.

The resulting energy gain is shown in Figure 11 for defects of $\Delta P = 1\%$ in a) (Chilean conditions) and d) (Norwegian conditions), $\Delta P = 10\%$ in b) (Chilean conditions) and e) (Norwegian conditions), and $\Delta P = 33\%$ in c) (Chilean conditions) and f) (Norwegian conditions). The peak of the curves, representing the maximum gain, is marked with a dot. The cost of replacing the modules, converted to kWh, is shown as black lines for feed-in tariff prices of 0.05, 0.1, and 0.5 €/kWh.

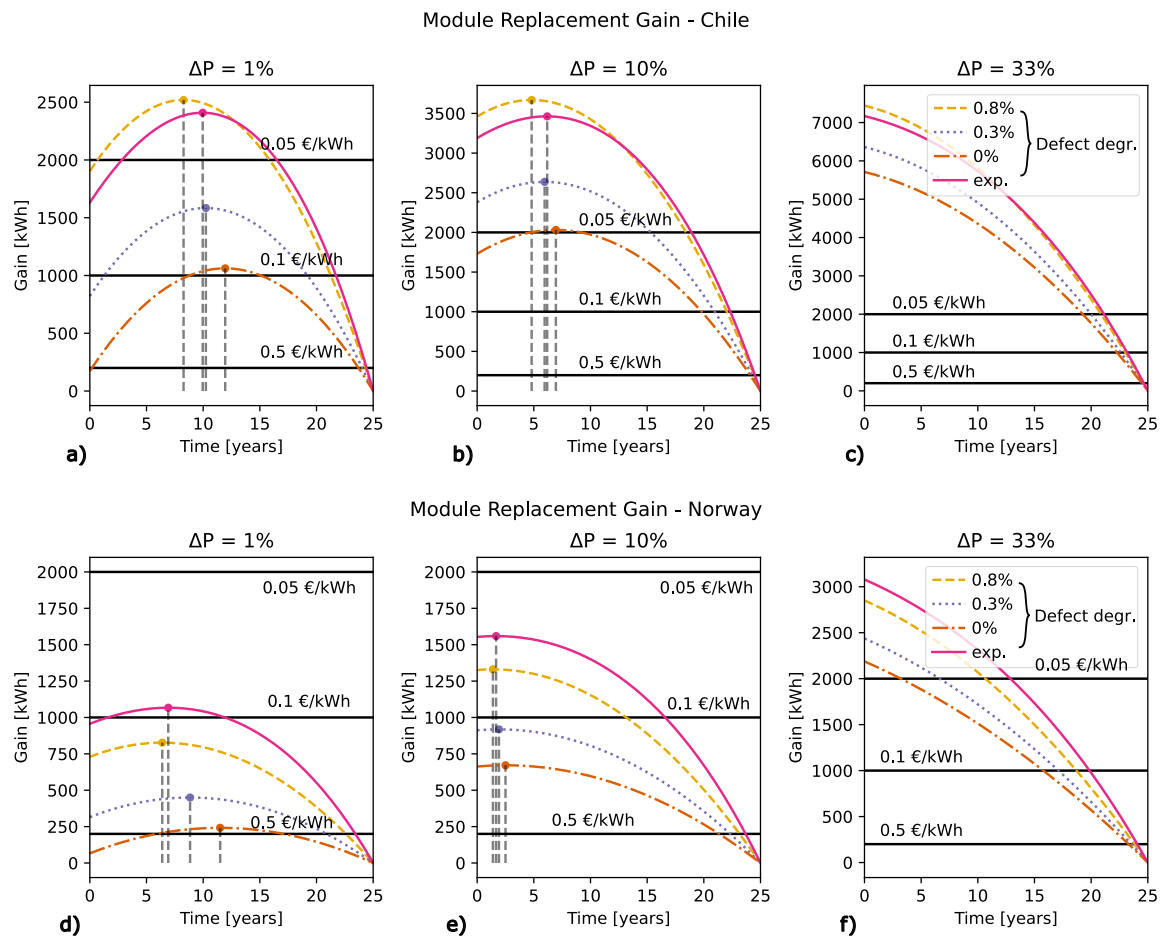


Figure 11. Module replacement gain for different defects ΔP and degradation rates. Conditions representative for Chile are shown in a), b) and c), and Norwegian conditions in d), e), and f). The horizontal lines show the cost of module replacement converted to kWh, for three different feed-in tariffs of 0.05, 0.1, and 0.5 €/kWh.

The general trends from the figures tell us that:

- The most cost-effective approach is not necessarily to replace a defective module immediately - for the less severe defects, the peak occurs after some years of degradation.
- The more significant the defects, the earlier the modules need to be replaced to ensure cost-effectiveness.
- The minor defect of $\Delta P = 1\%$ is most probably not cost-effective to replace in Norway, unless the feed-in tariff prices are as high as 0.5 €/kWh. For Chile it can be beneficial to replace the module, but mainly if the module has sustained around 10 years of additional module degradation before it is replaced with a new module.
- The medium size defect with a loss of $\Delta P = 10\%$ is cost-effective to replace in Chile, especially after around five years of additional module degradation, but might not be cost-effective to replace in Norway.
- The bypassed substring with a defect loss of $\Delta P = 33\%$ is cost-effective to replace in both Norway and Chile, even if they are discovered late in the park life.

6.2.2. Mid-Life Failures

The cost-effectiveness of replacing defective modules will depend on when the defects occur. This section will evaluate whether it is beneficial to replace modules with defects that appear mid-life. Figure 12 illustrates a scenario where a defect with power loss ΔP occurs at time t_i . The module degrades gradually until the defect incident, where Figure 12 a) shows the subsequent defect degradation

as three different linear rates, and b) illustrates the exponential defect degradation rate. The green areas demonstrate the gain from replacing the modules at time t_r . This alters the module replacement gain, where Figure 13 shows a scenario where the defects occur halfway in the park life, at $t_i = 12.5$ years. Figure 13 a), b), and c) show a defect of 1%, 10%, and 33%, respectively, in Chilean conditions. Figure 13 d), e), and f) show the same defects at Norwegian conditions. The key findings from the figure are:

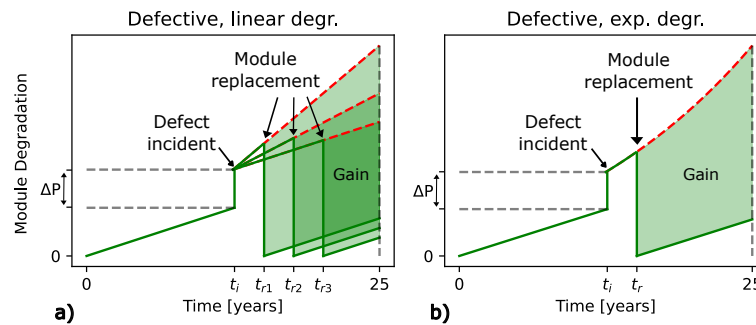


Figure 12. Illustration of a defect ΔP occurring at time t_i . a): three different linear defect degradation rates are shown, and b): an exponential defect degradation rate. The green areas illustrate the gain from module replacement at time t_r .

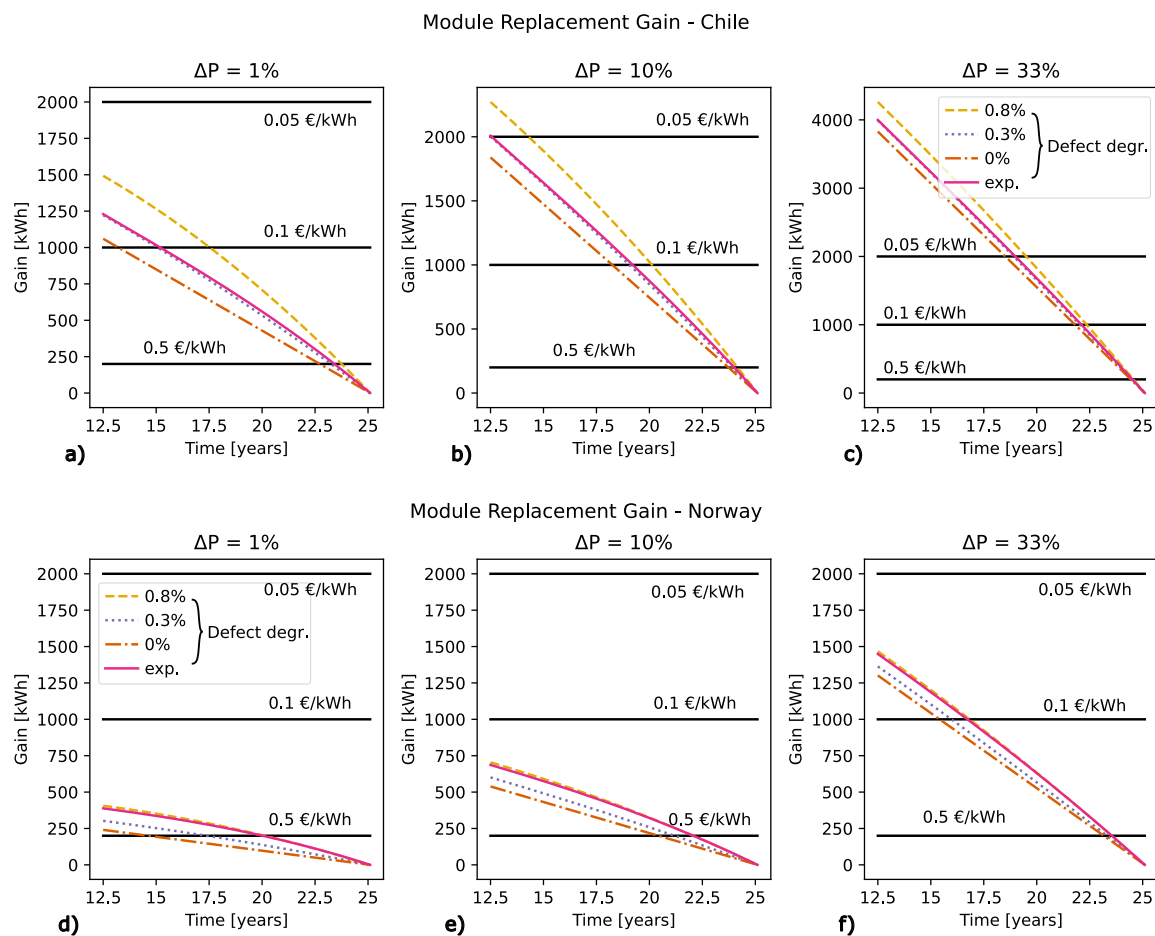


Figure 13. Module replacement gain for different defects ΔP occurring mid-life, after 12.5 years. The gain is shown for different defect degradation rates. Conditions representative for Chile are shown in a), b) and c), and Norwegian conditions in d), e), and f). The horizontal lines show the cost of module replacement converted to kWh, for three different feed-in tariffs of 0.05, 0.1, and 0.5 €/kWh.

- Unlike the infant-life failures in Figure 13, mid-life failures are most cost-effective to replace immediately.
- Minor defects of 1% are most likely not cost-effective to replace, even in high-irradiation locations like Chile.
- Defects of 10% are likely beneficial to replace mid-life in high-irradiation conditions, but not in low-irradiation locations like Norway.
- For the more severe defect of 33%, there is a substantial gain from replacing the module in high-irradiation locations, even when they are not immediately detected. There might be a gain from replacing the 33% defect in low-irradiation conditions as well, given an early detection.

One additional aspect of mid-life O&M is that a module replacing a defective one after more than 10 years of operation will likely have a higher capacity, due to technological advancements, and a lower cost from the increasing manufacturing. This gives an additional gain that would support the case for mid-life module replacement.

7. Summary and Conclusions

For this study, we established a test site with defective modules at Kjeller, Norway, as a foundation for assessments on the cost-effectiveness of module replacement. We demonstrated how the power loss from field-retrieved defects can be estimated based on thermal imagery, using a known defect as a reference. With the measured and estimated defect power losses, the long-term impact on the

power production is calculated both for low irradiation locations like Norway, and for high-irradiation countries like Chile. The first scenario assumed that the module defects were present from early park life. The cumulative power loss from the defect, defect degradation, and module degradation was used to calculate the energy gain from replacing the module at different times during a 25 years park lifetime. To assess whether replacing the module is cost-effective, the energy gain from module replacement is compared with the replacement cost, and the energy selling price.

The main findings is that for defects present from early-life, even minor defects are cost-effective to replace in high-irradiation locations. The timing is however crucial: The most significant benefits are achieved when the minor defects are replaced after approximately half of the park's lifespan, as the degradation at this point is considerable. This leads to a substantial increase in yield when replacing it with a new module. For more severe defects, an earlier replacement is more favorable. For low-irradiation locations, the cost-effectiveness of replacing defective modules is uncertain, unless the defect is as severe as a bypassed substring with its associated loss of 33%.

In the second scenario, the defects occurred mid-life, after 12.5 years. In this case, the minor defects of 1% have an uncertain cost-effectiveness associated with module replacement at high-irradiation locations, while for medium defects of 10% and severe defects of 33%, the gain is likely substantial. In low-irradiation locations, the substring defect is most likely the only cost-effective module to replace out of the three example defects.

We have thus seen that there might be a substantial gain from replacing defective modules, depending on the severity of the defect, but finding the optimal replacement time is crucial the cost-effectiveness.

Funding: This research received no external funding.

Author Contributions: Conceptualization, Victoria Lofstad-Lie; Data curation, Bjørn Aarseth and Nathan Roosloot; Formal analysis, Victoria Lofstad-Lie; Methodology, Victoria Lofstad-Lie and Bjørn Aarseth; Supervision, Bjørn Aarseth, Erik Marstein and Torbjørn Skauli; Visualization, Victoria Lofstad-Lie; Writing – original draft, Victoria Lofstad-Lie.

Data Availability Statement: Available upon request.

Conflicts of Interest: The authors declare no conflicts of interest.

Appendix A

In order to find the function that describes the defect degradation rate in Figure A1 a) from [13], the authors extracted three coordinates, marked in the figure, and performed a curve fitting. The fitted curve, shown as module degradation as opposite the module gain, is shown in Figure A1 with the associated function. It can be noted that reading out the coordinates from the graph might lead to slight inaccuracies, which will affect the obtained function.

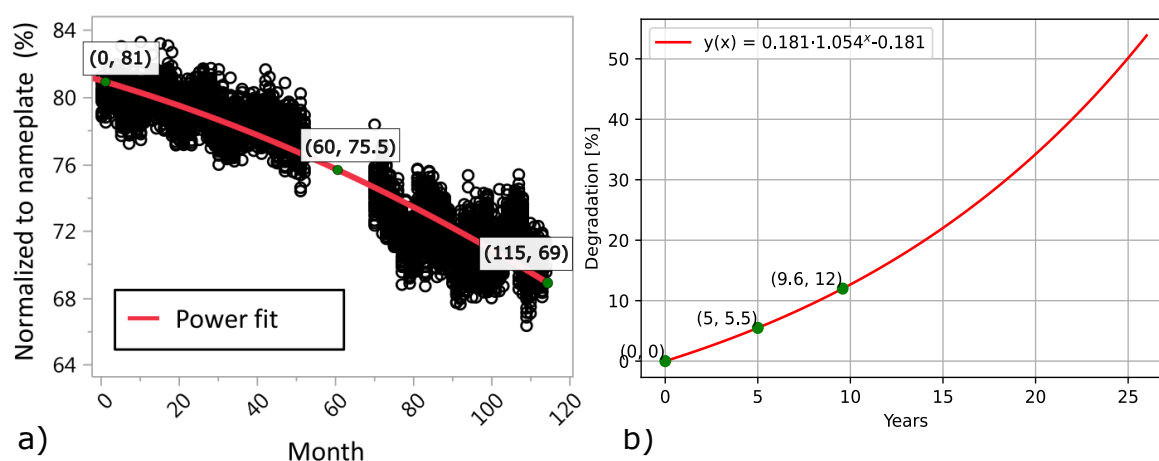


Figure A1. a) figure from [13] (coordinates added by author) of yield of a defective module, b) defect degradation based on curve fitting of coordinates from a)

References

1. Li, L.; Lin, J.; Wu, N.; Xie, S.; Meng, C.; Zheng, Y.; Wang, X.; Zhao, Y. Review and outlook on the international renewable energy development, 2022. doi:10.1016/j.enbenv.2020.12.002.
2. International Renewable Energy Agency. Renewable power generation costs in 2022. Technical report, 2023.
3. Mahdi, A.; Leahy, H.; Alghoul, P.G.; Morrison, M.; Al Mahdi, H.; Leahy, P.G.; Alghoul, M.; Morrison, A.P. A Review of Photovoltaic Module Failure and Degradation Mechanisms: Causes and Detection Techniques. *Solar* 2024, Vol. 4, Pages 43-82 **2024**, 4, 43–82. doi:10.3390/SOLAR4010003.
4. Rajput, P.; Singh, D.; Singh, K.Y.; Karthick, A.; Shah, M.A.; Meena, R.S.; Zahra, M.M.A. A comprehensive review on reliability and degradation of PV modules based on failure modes and effect analysis. *International Journal of Low-Carbon Technologies* **2024**, 19, 922–937. doi:10.1093/IJLCT/CTAD106.
5. Kim, J.; Rabelo, M.; Padi, S.P.; Yousuf, H.; Cho, E.C.; Yi, J. A review of the degradation of photovoltaic modules for life expectancy, 2021. doi:10.3390/en14144278.
6. Aghaei, M.; Fairbrother, A.; Gok, A.; Ahmad, S.; Kazim, S.; Lobato, K.; Oreski, G.; Reinders, A.; Schmitz, J.; Theelen, M.; Yilmaz, P.; Kettle, J. Review of degradation and failure phenomena in photovoltaic modules, 2022. doi:10.1016/j.rser.2022.112160.
7. Jordan, D.C.; Wohlgemuth, J.H.; Kurtz, S.R. Technology and climate trends in pv module degradation. *27th European Photovoltaic Solar Energy Conference and Exhibition* **2012**, pp. 3118–3124. doi:10.4229/27thEUPVSEC2012-4DO.5.1.
8. Dubey, R.; Chattopadhyay, S.; Kuthanazhi, V.; Kottantharayil, A.; Singh Solanki, C.; Arora, B.M.; Narasimhan, K.L.; Vasi, J.; Bora, B.; Singh, Y.K.; Sastry, O.S. Comprehensive study of performance degradation of field-mounted photovoltaic modules in India. *Energy Science and Engineering* **2017**, 5, 51–64. doi:10.1002/ese3.150.
9. Jordan, D.C.; Kurtz, S.R.; VanSant, K.; Newmiller, J. Compendium of photovoltaic degradation rates. *Progress in Photovoltaics: Research and Applications* **2016**, 24, 978–989. doi:https://doi.org/10.1002/pip.2744.
10. Singh, J.; Belmont, J.; TamizhMani, G. Degradation analysis of 1900 PV modules in a hot-dry climate: Results after 12 to 18 years of field exposure. 2013 IEEE 39th Photovoltaic Specialists Conference (PVSC), 2013, pp. 3270–3275. doi:10.1109/PVSC.2013.6745149.
11. Deceglie, M.G.; Silverman, T.J.; Member, S.; Young, E.; Hobbs, W.B.; Member, S.; Libby, C. Field and Accelerated Aging of Cracked Solar Cells. *IEEE Journal of Photovoltaics* **2023**, 13, 836–841. doi:10.1109/JPHOTOV.2023.3309933.
12. Suleske, A.; Singh, J.; Kuitche, J.; Tamizh-Mani, G. Performance degradation of grid-tied photovoltaic modules in a hot-dry climatic condition. Reliability of Photovoltaic Cells, Modules, Components, and Systems IV. SPIE, 2011, Vol. 8112, p. 81120P. doi:10.1117/12.894928.
13. Jordan, D.C.; Silverman, T.J.; Sekulic, B.; Kurtz, S.R. PV degradation curves: non-linearities and failure modes. *Progress in Photovoltaics: Research and Applications* **2017**, 25, 583–591. doi:10.1002/pip.2835.

14. Buerhop, C.; Wirsching, S.; Bemm, A.; Pickel, T.; Hohmann, P.; Nieß, M.; Vodermayr, C.; Huber, A.; Glück, B.; Mergheim, J.; Camus, C.; Hauch, J.; Brabec, C.J. Evolution of cell cracks in PV-modules under field and laboratory conditions. *Progress in Photovoltaics: Research and Applications* **2018**, *26*, 261–272. doi:10.1002/pip.2975.
15. International Electrotechnical Commission. Photovoltaic devices - Part 9: Solar simulator performance requirements. *IEC International Standard 60904-9* **2007**.
16. Holmgren, W.F.; Hansen, C.W.; Mikofski, M.A. pvlib python: a python package for modeling solar energy systems. *Journal of Open Source Software* **2018**, *3*, 884. doi:https://doi.org/10.21105/joss.00884.
17. Teubner, J.; Buerhop, C.; Pickel, T.; Hauch, J.; Camus, C.; Brabec, C.J. Quantitative assessment of the power loss of silicon PV modules by IR thermography and its dependence on data-filtering criteria. *Progress in Photovoltaics: Research and Applications* **2019**, *27*, 856–868. doi:10.1002/pip.3175.
18. Moretón, R.; Lorenzo, E.; Narvarte, L. Experimental observations on hot-spots and derived acceptance/rejection criteria. *Solar Energy* **2015**, *118*, 28–40. doi:10.1016/j.solener.2015.05.009.
19. Dhimish, M.; Badran, G. Investigating defects and annual degradation in UK solar PV installations through thermographic and electroluminescent surveys. *npj Materials Degradation* **2023**, *7*. doi:10.1038/s41529-023-00331-y.
20. National Solar Radiation Database: <https://nsrdb.nrel.gov/data-viewer>, 2024.
21. Solar module prices increase for first time in years, Anza reports – pv magazine USA: <https://pv-magazine-usa.com/2024/06/12/solar-module-prices-increase-for-first-time-in-years-anza-reports/>, 2014.
22. Feed-in tariffs (FITs) in Europe – pv magazine International: <https://www.pv-magazine.com/features/archive/solar-incentives-and-fits/feed-in-tariffs-in-europe/>, 2024.

Disclaimer/Publisher's Note: The statements, opinions and data contained in all publications are solely those of the individual author(s) and contributor(s) and not of MDPI and/or the editor(s). MDPI and/or the editor(s) disclaim responsibility for any injury to people or property resulting from any ideas, methods, instructions or products referred to in the content.